communications physics

ARTICLE

https://doi.org/10.1038/s42005-023-01337-3 OPEN

Formation of turing patterns in strongly magnetized electric discharges

Mohamad Menati [1✉], Stephen Williams[1], Behnam Rasoolian[2], Edward Thomas Jr. [1] & Uwe Konopka [1]

Pattern formation and self-organization in many biological and non-biological systems can be explained through Turing's activator-inhibitor model. Here we show how this model can be employed to describe the formation of filamentary structures in a low-pressure electric discharge exposed to a strong magnetic field. Theoretical investigation reveals that the fluid equations describing a magnetized plasma can be rearranged to take the mathematical form of Turing's activator-inhibitor model. Numerical simulations based on the equations derived from this approach could reproduce the various patterns observed in the experiments. Also, it is shown that a density imbalance between electrons and ions exists in the bulk of the magnetized plasma that generates an electric field structure transverse to the applied magnetic field. This electric field is responsible for the stability of the filamentary patterns in the magnetized plasma over time scales much longer than the characteristic time scales of the electric discharge.

[1] Physics Department, Auburn University, Auburn, AL 36849, USA. [2] Department of Computer Science and Software Engineering, Auburn University, Auburn, AL 36849, USA. ✉email: mzm0085@auburn.edu

Due to the nonlinear nature of electric discharges, they possess an extensive capability for supporting self-organization and pattern formation and consequently, these phenomena have been reported in various plasma systems[1–13]. In this context, patterns in a plasma are defined as regions within the discharge that are different from the rest of the plasma in terms of properties such as optical brightness and density. The study of self-organization in plasmas is important not only from the phenomenological point of view to discover the physics behind the phenomenon but also, due to its technological applications. Pattern formation in electric discharges can be favorable in the process of nanoparticle synthesis[14,15], plasma etching[16,17], localized heating[13], and surface treatment[18,19]. On the other hand, if the self-organized patterns result in decreasing the electrodes life, or nonuniformity and defects in the surface of the substrates under treatment, they are extremely undesirable[4,13,20,21].

Plasma systems at different operating conditions have been observed to support pattern formation; including high-power high-pressure, high-power low-pressure, low-power low-pressure, and low-power high-pressure discharges[13]. Of particular interest to this work is the formation of three-dimensional (3D) filamentary structures in strongly magnetized ($B > 1$T) low-pressure electric discharges (filamentation phenomenon)[22–27]. Neutral gas pressure and magnetic field strength are the most influential parameters on the properties of filamentation phenomenon where the patterns tend to disappear at high pressures or low magnetic fields. As an example, for the specific geometry of our set up[28,29], the filamentary patterns do not form in the discharge exposed to 1 T magnetic field if the neutral gas pressure is of the order $P > 20$ Pa. Moreover, depending on the discharge properties, different shapes of filamentary structures can form in the magnetized plasma.

Figure 1 shows the formation of filamentary patterns in a strongly magnetized Argon plasma and their variation with different discharge parameters. The appearance of these various filamentary patterns including concentric rings, spirals, maze-like, and individual spots suggests that there is a complex formation mechanism for them. Figure 1f shows a side view of the filamented plasma, i.e., the magnetic field is pointing from the top to the bottom of this image while in Fig. 1a–e, the magnetic field direction is into the page. Therefore, the filamentary structures extend vertically into the plasma along the magnetic field. All of these images were taken from experiments performed using the Magnetized Dusty Plasma Experiment (MDPX) device at Auburn University[28,29]. The MDPX device consists of two parallel plate electrodes which are 30.5 cm in diameter and there is a gap of 6.3 cm between them. To generate a capacitively coupled plasma (CCP), the bottom electrode is grounded while the top electrode is powered at an RF frequency of 13.56 MHz. A background magnetic field is applied, oriented perpendicular to the electrodes. The plasma is observed through a 15 cm diameter view port at the top of the vacuum chamber[28,29].

Despite being known for over a decade, there has been no explanation for filamentation phenomenon. Therefore, finding an explanation for the formation and stability mechanism of this phenomenon would be a big step towards better understanding of charged particles transport in strongly magnetized plasmas. In the current work, we show that magnetized low-pressure plasmas can be categorized under activator-inhibitor systems, which are understood to support self-organization[30]. In such systems, the activator amplifies the production of both the inhibitor and itself while the inhibitor suppresses the production of the activator[31]. Moreover, the inhibitor diffuses faster than the activator in such systems.

It will be also shown that the presence of the strong magnetic field in the discharge and its effect on the cross-field transport of the charged species imposes the activator-inhibitor properties on the electrons and ions. In this context, the electrons, which are the main source of ionization through collision with neutral atoms, will be the activator and the ions that can spread faster than the electrons in the cross-field direction will be the inhibitor.

In the current work, we not only show that pattern formation in magnetized plasmas can be explained through Turing's activator-inhibitor model but also discuss the underlying physics behind their long-term stability. It is illustrated that the presence of the strong magnetic field in the discharge causes a density imbalance between electrons and ions in the filamentary structures. This density imbalance results in a plasma potential profile and consequently an electric field structure that maintains the filamentary patterns over time scales much longer than the characteristic time scales of the plasma.

Results and discussion

Formation of self-organized structures in magnetized plasmas as an activation-inhibition process. Activator-inhibitor is the two-component class of the reaction-diffusion model for self-organization which was proposed in 1952 by Allan Turing as a basis for morphogenesis[30]. The two components of activator-inhibitor systems have different diffusion rates, and the inhibitor diffuses faster than the activator[30]. Also, the activator amplifies the production of both species (activation and autocatalysis) while the inhibitor slows down the growth of the activator to bring the system to an equilibrium (inhibition)[32–34]. Figure 2 shows a schematic drawing of an activator-inhibitor system in which the activator has a positive feedback on the inhibitor but the feedback of the inhibitor on the activator is negative. It has been shown that a system exhibiting these behaviors can support self-organization and the model has been successfully adopted to explain the pattern formation process in a variety of geographical, biological, chemical, and physical entities[35–45].

The activator-inhibitor model can be expressed using two coupled partial differential equations (PDEs) through which the time variations of the activator and inhibitor concentrations are given as functions of the concentrations and position[30,46]:

$$\frac{\partial n_a}{\partial t} = f(n_a, n_i) + \Omega_a \nabla^2 n_a \tag{1}$$

$$\frac{\partial n_i}{\partial t} = g(n_a, n_i) + \Omega_i \nabla^2 n_i \tag{2}$$

in which n_a is concentration of the activator, n_i is concentration of the inhibitor, and Ω_a & Ω_i are isotropic diffusion coefficients of the activator and inhibitor, respectively ($\Omega_i \gg \Omega_a$). The functions $f(n_a, n_i)$ and $g(n_a, n_i)$ carry the expressions of amplification and inhibition.

There are extended versions of Turing's framework for pattern formation that predict self-organization through scenarios that are not anticipated by the classical activator-inhibitor model[47–51]. In particular, Busiello et al.[51] propose a mathematical model for pattern formation in an activator-inhibitor system undergoing anisotropic diffusion. The general form of Busiello model in the two-dimensional (2D) space for species of n_a (activator) and n_i (inhibitor) reads:

$$\frac{\partial n_a}{\partial t} = f(n_a, n_i) + D_a^x \frac{\partial^2 n_a}{\partial x^2} + D_a^y \frac{\partial^2 n_a}{\partial y^2} \tag{3}$$

$$\frac{\partial n_i}{\partial t} = g(n_a, n_i) + D_i^x \frac{\partial^2 n_i}{\partial x^2} + D_i^y \frac{\partial^2 n_i}{\partial y^2} \tag{4}$$

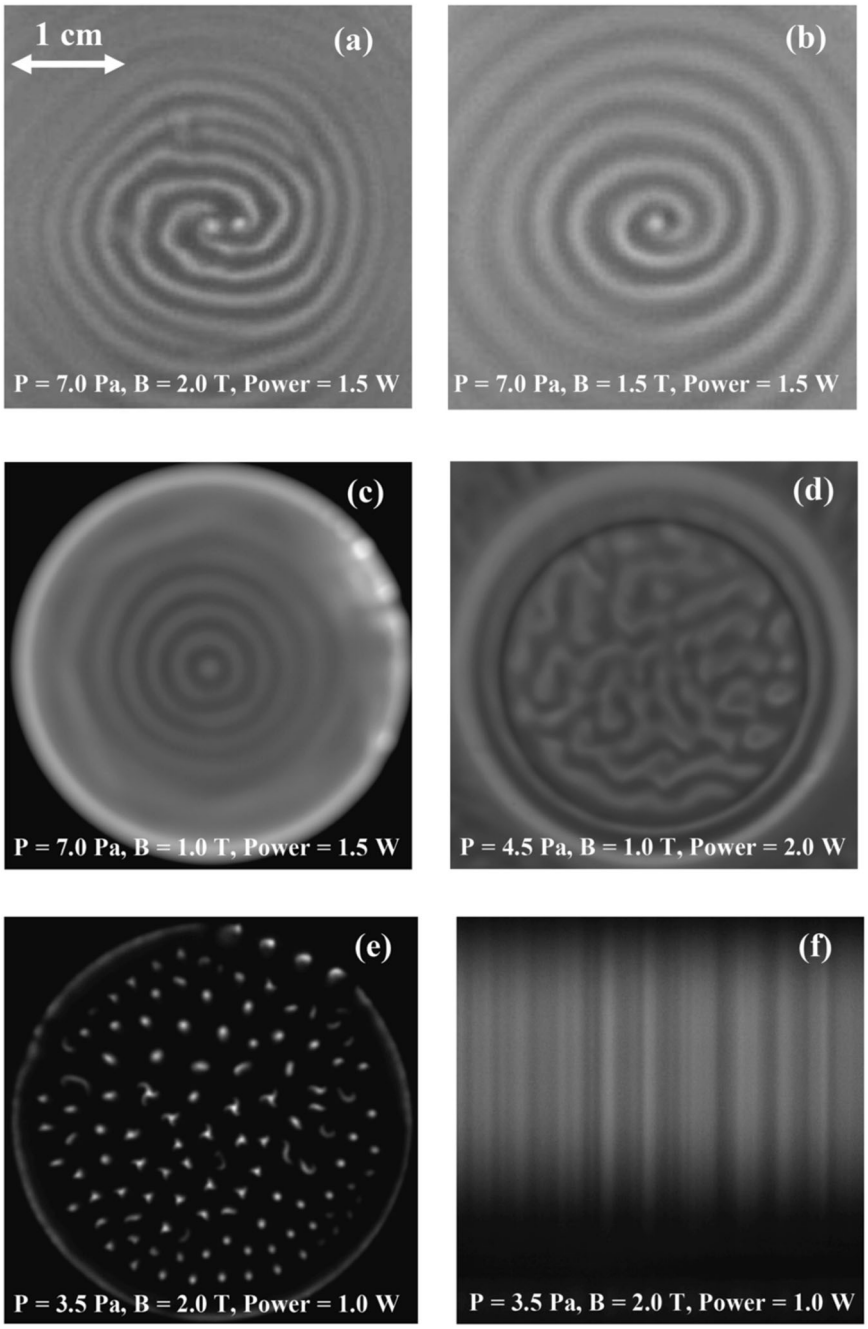

Fig. 1 Different filamentary patterns observed in a magnetized Argon plasma under different operating conditions in the MDPX device at Auburn University. Operating conditions are displayed on each pattern in which P stands pressure and B stands for magnetic field strength. **a**–**e** display the top-view of the experiment, and (**f**) displays the side-view for the pattern observed in **c**. In **a**–**e**, the magnetic field direction is into the page, while it is pointing from the top to the bottom in **f**. The scale of the pictures is shown in the upper left corner of **a**.

in which D_a^x & D_i^x are diffusion coefficients along X axis, D_a^y & D_i^y are diffusion coefficients along Y axis, and $f(n_a, n_i)$ & $g(n_a, n_i)$ carry the expressions of amplification and inhibition. Along other circumstances that could lead to pattern formation, Busiello et al. have shown that a system in which $D_i^x > D_a^x$ while $D_i^y < D_a^y$ will be capable of supporting self-organized patterns that are extended along Y axis[51].

In the presence of strong magnetic field, the electrons Larmor radius is so small that they practically cannot diffuse across the magnetic field lines. On the other hand, the ions that are much heavier than the electrons have a much larger Larmor radius that enables them to have a limited diffusion across the magnetic field lines. Moreover, in the direction parallel to the magnetic axis, the dynamics of the electrons and ions will not be affected by the magnetic field, and electrons can move much faster than the ions. In magnetized electric discharges, the directions perpendicular and parallel to the applied magnetic field can be assumed to correspond to X and Y directions in the Busiello model. Therefore, this model appears to be suitable for describing the formation of filamentary patterns in strongly magnetized plasmas.

In order to derive the mathematical framework that describes a magnetized plasma as an activator-inhibitor system, we start with the continuity equation that gives the time variation of the

electron/ion densities:

$$\frac{\partial n_\alpha}{\partial t} + \nabla \cdot \boldsymbol{\Gamma}_\alpha = I - R \tag{5}$$

where n_α is the density of each species α (= e, i - for electrons and ions), $\boldsymbol{\Gamma}_\alpha$ is the flux vector of each species α, I is the ionization rate, and R is recombination rate of the electrons and ions.

For an isothermal plasma in the presence of a magnetic field, the fluxes of electrons/ions in the directions perpendicular and parallel to the magnetic axis are given by[52,53]:

$$\boldsymbol{\Gamma} = \pm \mu_{\alpha\perp} n_\alpha \mathbf{E}_\perp - D_{\alpha\perp} \nabla_\perp \boldsymbol{n}_\alpha + \frac{\boldsymbol{\Gamma}_{\alpha E} + \boldsymbol{\Gamma}_{\alpha D}}{1 + \frac{\upsilon_\alpha^2}{\omega_{c\alpha}^2}} \tag{6}$$

$$\boldsymbol{\Gamma}_{||} = \pm \mu_{\alpha||} n_\alpha \mathbf{E}_{||} - D_{\alpha||} \nabla_{||} \boldsymbol{n}_\alpha \tag{7}$$

in which, for each species α (electrons or ions), μ_α is mobility, $\mathbf{E}_\perp$ is the cross-field component of electric field, $\mathbf{E}_{||}$ is the component of electric field parallel to the magnetic field, D_α is diffusion coefficient, $\nabla_\perp \mathbf{n}$ is gradient of density in cross-field direction, $\nabla_{||} \mathbf{n}$ is gradient of density parallel to the magnetic field, $\boldsymbol{\Gamma}_{\alpha \mathbf{E}}$ is the flux due to $\mathbf{E}\times\mathbf{B}$ drift[52,53], $\boldsymbol{\Gamma}_{\alpha \mathbf{D}}$ is the flux due to diamagnetic drift ($\nabla \mathbf{n}\times\mathbf{B}$)[52,53], υ_α is collision frequency with neutral gas atoms, and $\omega_{c\alpha}$ is cyclotron frequency. Also, in the first terms, the "+" sign applies to the ions, and the "-" sign applies to the electrons.

The anisotropic coefficients of mobility and diffusion, the flux due to $\mathbf{E}\times\mathbf{B}$ drift, and the flux due to diamagnetic drift are defined below:

$$\mu_{\alpha_{||}} = \frac{q_\alpha}{m_\alpha \upsilon_\alpha} \tag{8}$$

$$D_{\alpha_{||}} = \frac{K_b T_\alpha}{m_\alpha \upsilon_\alpha} \tag{9}$$

$$\mu_{\alpha_\perp} = \frac{\mu_{\alpha_{||}}}{1 + \frac{\omega_{c\alpha}^2}{\upsilon_\alpha^2}} \tag{10}$$

$$D_{\alpha_\perp} = \frac{D_{\alpha_{||}}}{1 + \frac{\omega_{c\alpha}^2}{\upsilon_\alpha^2}} \tag{11}$$

$$\boldsymbol{\Gamma}_{\alpha E} = n_\alpha \frac{\mathbf{E}\times\mathbf{B}}{B_0^2} \tag{12}$$

$$\boldsymbol{\Gamma}_{\alpha D} = -\frac{K_b T_\alpha}{q_\alpha B_0^2} \nabla \mathbf{n}\times\mathbf{B} \tag{13}$$

where, for each species of plasma, m_α is mass, q_α is electric charge, T_α is temperature, K_b is Boltzmann constant and B_0 is the magnitude of the applied magnetic field.

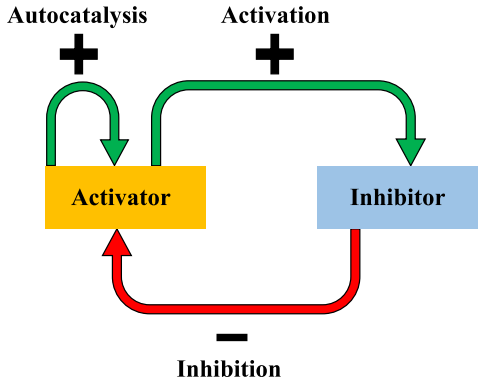

Fig. 2 Schematic drawing of activator-inhibitor model. In this model the activator accelerates the production of the inhibitor (activation) and itself (autocatalysis), but the inhibitor decelerates the production of the activator (inhibition). This process can lead to self-organization and pattern formation.

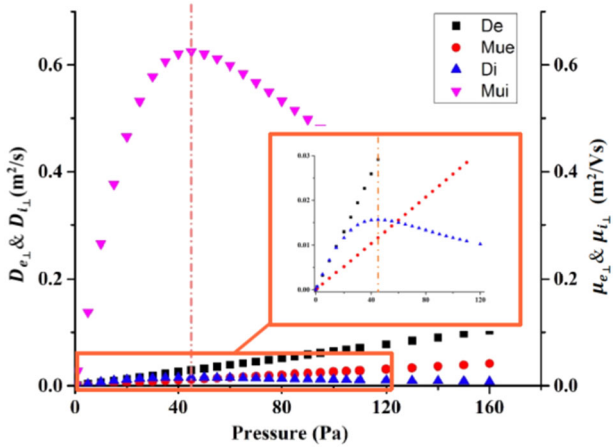

Fig. 3 The variation of cross-field mobility and diffusion coefficients of the electrons and ions with pressure, for magnetized Argon plasma exposed to 1.0 T magnetic field. In this figure, $D_{e\perp}$ is electron diffusivity, $D_{i\perp}$ is ion diffusivity, $\mu_{e\perp}$ is electron mobility, and $\mu_{i\perp}$ is ion mobility in the direction perpendicular to the magnetic field orientation. The electron and ion temperatures are assumed to be 2.5 eV and 0.025 eV, respectively. The vertical dashed line placed on the graphs indicates the critical pressure beyond which the filamentary patterns do not form in the simulated plasma for the aforementioned discharge parameters.

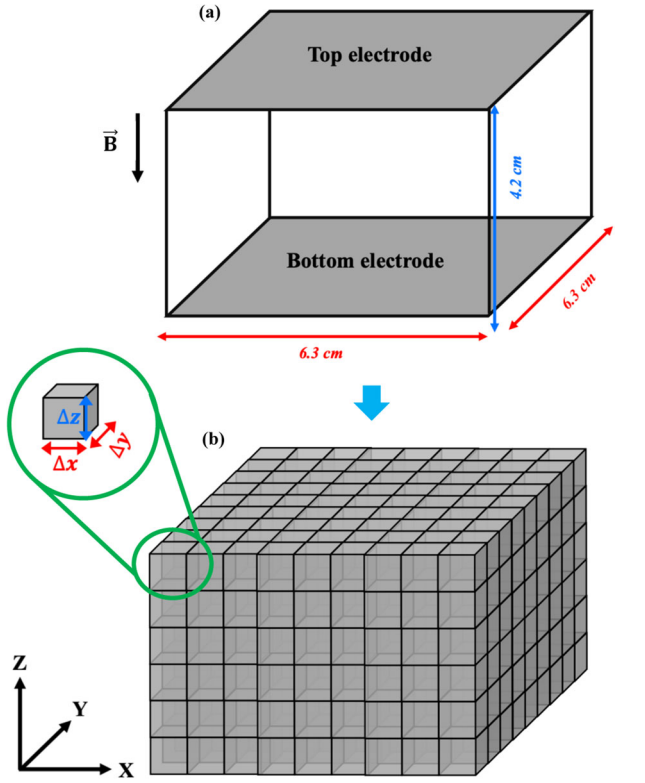

Fig. 4 The computational space and its discretization in REMAPS code. **a** Schematic drawing of the rectangular plasma chamber considered in the code for the simulations of filamentary patterns in magnetized plasmas, and (**b**) the corresponding discretization of the computational space in cartesian coordinate system.

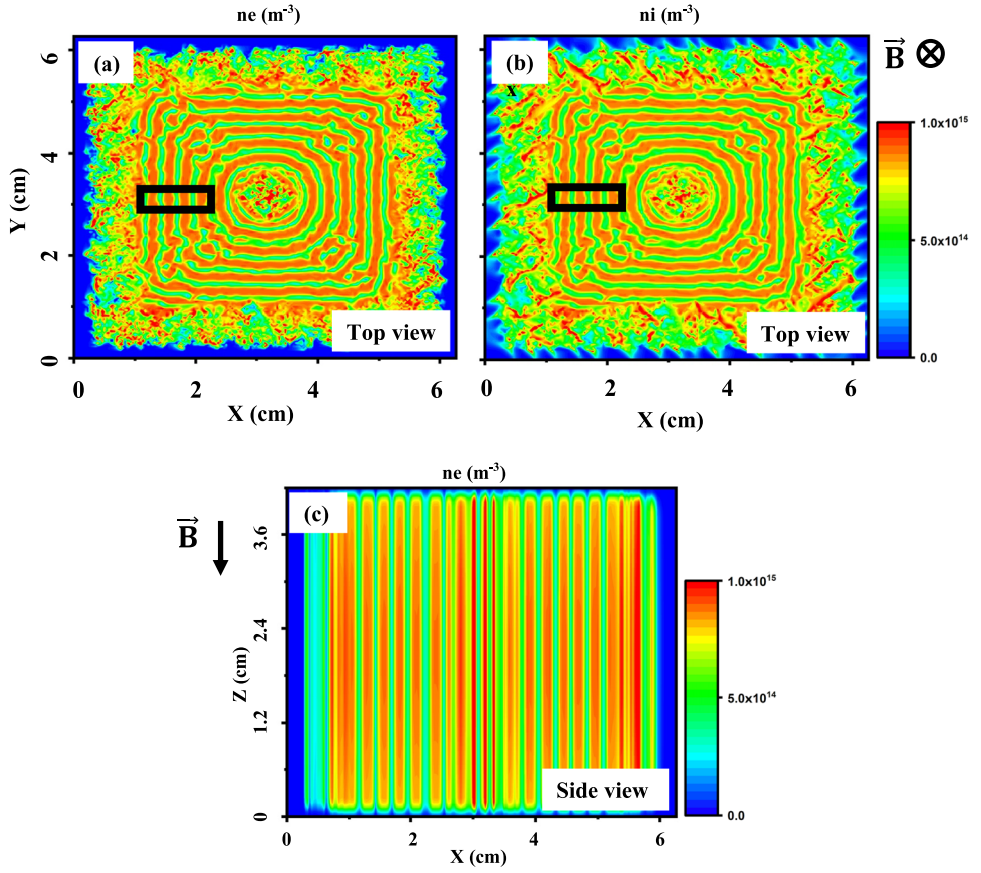

Fig. 5 The simulation results for filamentation phenomenon in magnetized Argon plasma. a Top-view of the electron density profile (n_e), (**b**) top-view of the ion density profile (n_i), and (**c**) side-view of the electron density profile (the color bars next to the graphs represent the magnitude of the densities). The plasma gas was Argon. The initial uniform plasma density was assumed to be 5.0×10^{14} m^{-3}, the neutral pressure was 9.0 Pa, electron temperature was 2.5 eV, ion temperature was 0.025 eV, and the magnetic field strength (**B**) was 1.0 T applied in negative Z direction. The electron and ion density profiles seem to be similar, and the filamentary patterns are extended in the plasma parallel to the applied magnetic field. These results are consistent with the experimental observation presented in Fig. 1. The regions enclosed in the black boxes on the top-view graphs are magnified and explained in the next figures.

As mentioned, the magnetic field does not affect the behavior of plasma along the magnetic axis. Therefore, the parallel component of the electric field in the bulk of the magnetized plasma (away from the sheath regions) is very weak and it can be neglected compared to the electric field component perpendicular to the magnetic field ($\mathbf{E}_{\parallel} \ll \mathbf{E}_{\perp}$)[52,53]. Plugging the fluxes from Eqs. 6 and 7 into Eq. 5 and doing simple vector algebra yields:

$$\frac{\partial n_\alpha}{\partial t} = I - R \mp \mu_{\alpha\perp} n_\alpha \nabla \cdot \mathbf{E}_\perp \mp \mu_{\alpha\perp} \mathbf{E}_\perp \cdot \nabla_\perp \boldsymbol{n_\alpha} + D_{\alpha\perp} {\nabla_\perp}^2 n_\alpha + D_{\alpha_\parallel} {\nabla_\parallel}^2 n_\alpha \tag{14}$$

Since the component of electric field parallel to the magnetic axis is equal to zero, Poisson's equation can be written as:

$$\nabla \cdot \mathbf{E}_\perp = \nabla \cdot \mathbf{E} = \frac{q_i n_i - e n_e}{\varepsilon_0} \tag{15}$$

in which, **E** is the electric field, e is the unit charge, q_i is the charge of the ions, and ε_0 is the electric permittivity of free space.

By plugging in from Eq. 15, Eq. 14 becomes:

$$\frac{\partial n_\alpha}{\partial t} = I - R \mp \mu_{\alpha\perp} n_\alpha \left(\frac{q_i n_i - e n_e}{\varepsilon_0}\right) \mp \mu_{\alpha\perp} \mathbf{E}_\perp \cdot \nabla_\perp \mathbf{n_\alpha} + D_{\alpha\perp} {\nabla_\perp}^2 n_\alpha + D_{\alpha_\parallel} {\nabla_\parallel}^2 n_\alpha \tag{16}$$

In a weakly ionized plasma (ionization fraction of the order $\leq 10^{-6}$), similar to the electric discharges in the MDPX, the ionization and recombination rate of the electrons and ions can be written as[52,53]:

$$I = \eta n_e \tag{17}$$

$$R = \chi n_e n_i \tag{18}$$

where, η and χ are coefficients of ionization and recombination, respectively. To view the plasma as an activator-inhibitor system, the ionization term in the fluid equations of plasma ($I = \eta n_e$) can be considered as the activation and autocatalysis mechanism by the electrons, i.e., upon the collision of electrons with the neutral gas atoms an electron/ion pair can be produced. Also, the recombination term ($R = \chi n_e n_i$) can be assumed as the inhibition mechanism.

By plugging Eqs. 17 and 18 into Eq. 16 for electrons and ions, we get the final form of continuity equation for magnetized plasma as:

$$\frac{\partial n_e}{\partial t} = \eta n_e - \frac{\mu_{e\perp} e}{\varepsilon_0} {n_e}^2 - \left(\chi - \frac{\mu_{e\perp} q_i}{\varepsilon_0}\right) n_e n_i + \mu_{e\perp} \mathbf{E}_\perp \cdot \nabla_\perp \mathbf{n_e} + D_{e\perp} \nabla^2 n_e + D_{e_\parallel} {\nabla_\parallel}^2 n_e \tag{19}$$

$$\frac{\partial n_i}{\partial t} = \eta n_e - \frac{\mu_{i\perp} q_i}{\varepsilon_0} {n_i}^2 - \left(\chi - \frac{\mu_{i\perp} e}{\varepsilon_0}\right) n_e n_i - \mu_{i\perp} \mathbf{E}_\perp \cdot \nabla_\perp \mathbf{n_i} + D_{i\perp} \nabla^2 n_i + D_{i_\parallel} {\nabla_\parallel}^2 n_i \tag{20}$$

By considering the first few terms on the right-hand side of these equation as activation/inhibition functions, these equations

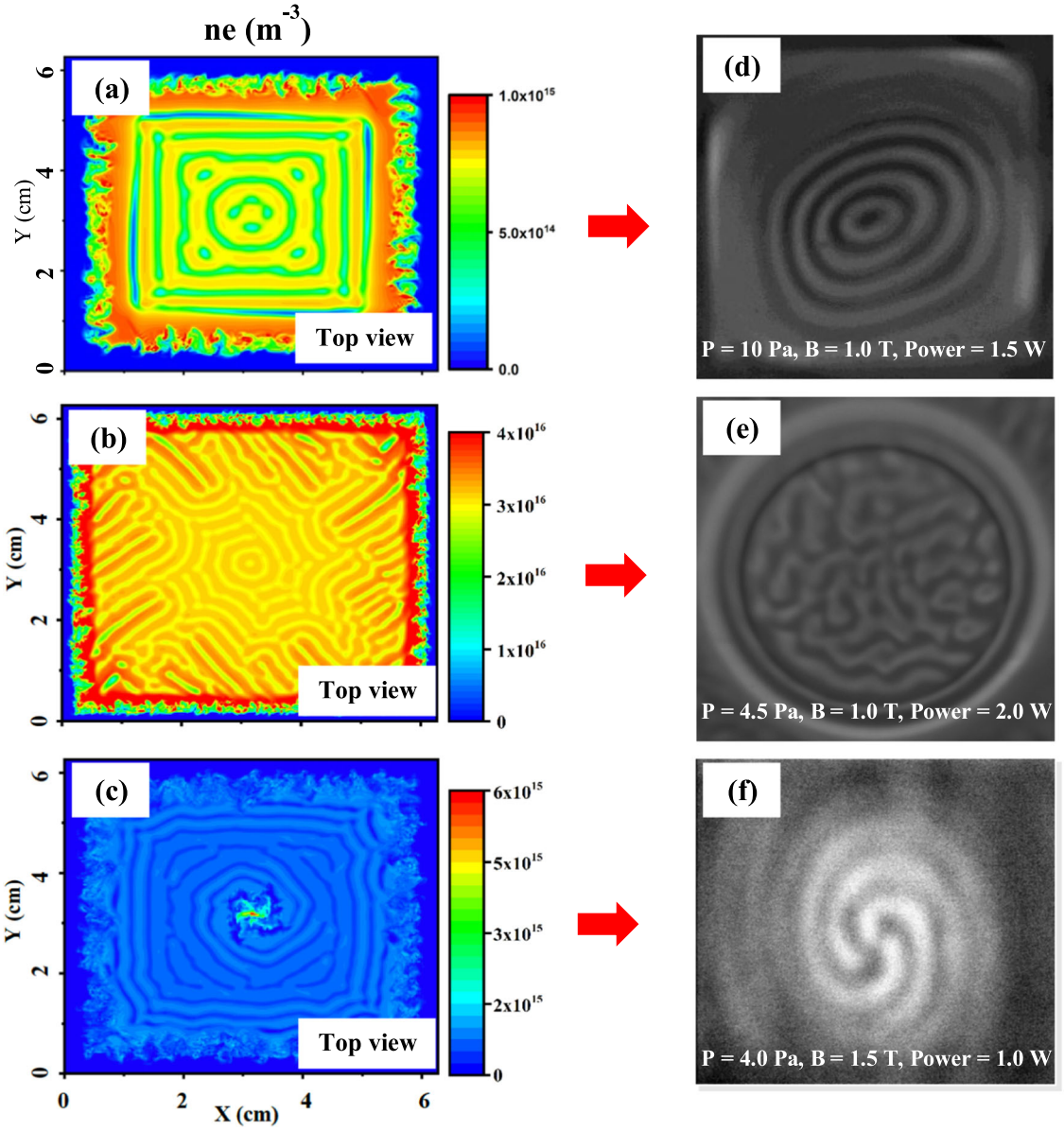

Fig. 6 Formation of different filamentary pattern in the simulation of filamentation phenomenon in magnetized Argon plasma by varying different plasma parameters and the similar patterns observed in the experiments. It has to be noted that we are not directly simulating any of the experiments and they are only displayed side by side to emphasize the resemblance of the patterns. The electron temperature in the simulations was 2.5 eV, and ion temperature was 0.025 eV. In **a**, the initial plasma density was 5.0×10^{14} m^{-3}, the neutral gas pressure was 12.0 Pa, and the magnetic field strength was 0.8 T. In **b**, the initial plasma density was 5.0×10^{15} m^{-3}, the neutral pressure was 6.0 Pa, and the magnetic field strength was 1.0 T. In **c**, the initial plasma density was 5.0×10^{14} m^{-3}, the neutral gas pressure was 5.0 Pa, the magnetic field strength was 1.0 T, and a high-density column as a perturbation was added at the center of the plasma chamber. The color bars next to the simulation graphs represent the magnitude of the electron density. The discharge parameters in the experimental figures (**d**–**f**) are displayed on each figure in which P stands pressure and B stands for magnetic field strength. In general, changing the initial condition in the simulations can result in the formation of a different filamentary pattern as variation of the discharge parameters in the experiment would have the same effect.

can be re-written as:

$$\frac{\partial n_e}{\partial t} = f(n_e, n_i) + \mu_{e\perp}\mathbf{E}\bullet\nabla\mathbf{n_e} + D_{e\perp}\nabla^2 n_e + D_{e_\parallel}\nabla_\parallel{}^2 n_e \qquad (21)$$

$$\frac{\partial n_i}{\partial t} = g(n_e, n_i) - \mu_{i\perp}\mathbf{E}\cdot\nabla\mathbf{n_e} + D_{i\perp}\nabla^2 n_i + D_{i_\parallel}\nabla_\parallel{}^2 n_i \qquad (22)$$

which have the exact same form as Eqs. 3 and 4 except for the drift terms for electrons and ions due to the presence of the electric field in the bulk of magnetized plasma ($\mu_{\alpha\perp}\mathbf{E}\cdot\nabla\mathbf{n_\alpha}$). It has to be noted that unlike other natural and controlled activator-inhibitor systems, the spreading of the particles in plasmas can occur not only due to gradient of density but also due to the presence of electric field. Also, the activation and inhibition functions ($f(n_e, n_i)$ and $g(n_e, n_i)$) derived in Eqs. 19–22 are similar to Segel-Jackson activator-inhibitor model which was introduced to describe the formation of dissipative patterns through predator-prey interactions[50].

The variation of cross-field mobility and diffusion coefficients of the electrons and ions with neutral gas pressure for a magnetized argon plasma exposed to 1.0 T magnetic field is shown in Fig. 3. This figure can be employed to demonstrate the analogy between Eqs. 21–22 and Eqs. 3–4. It can be seen in this

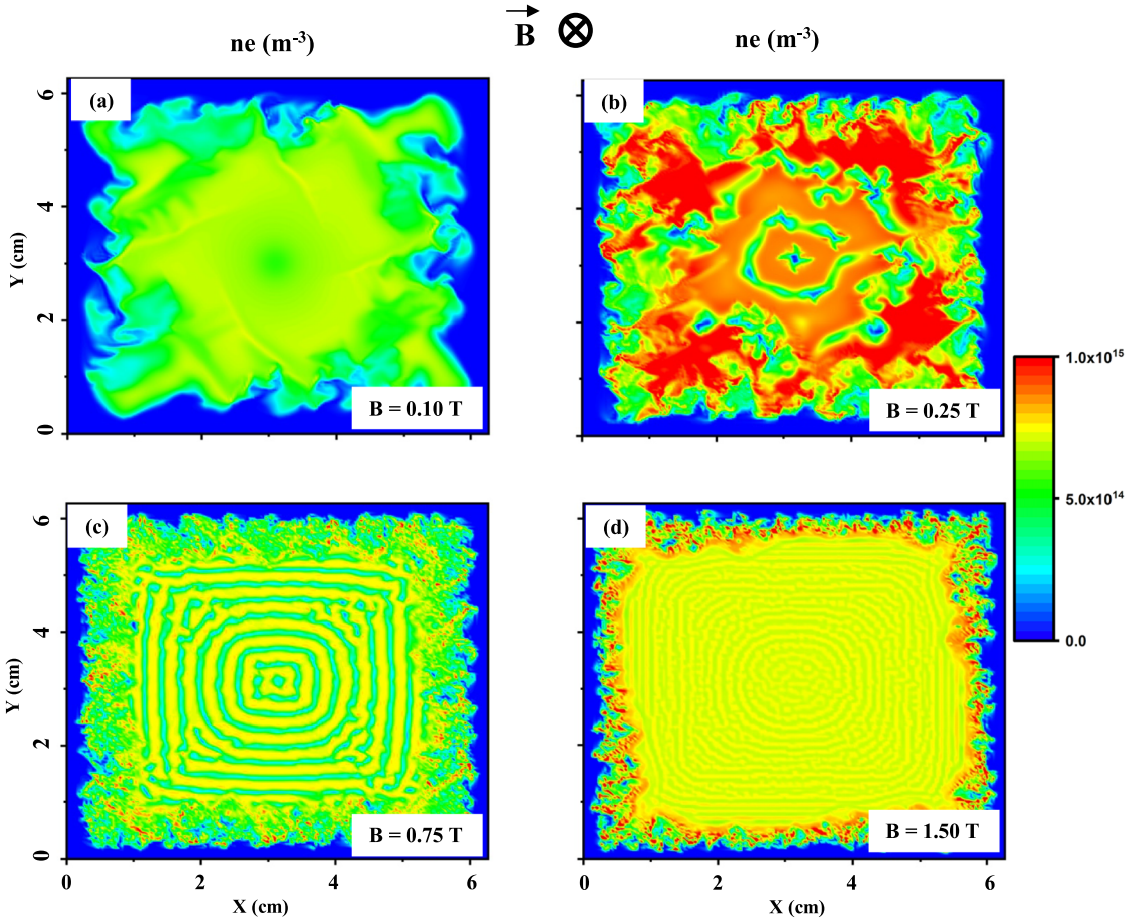

Fig. 7 X-Y cross section of the electron density profile in the simulation of an argon plasma exposed to different magnetic fields (B). a 0.10 T, (**b**) 0.25 T, (**c**) 0.75 T, (**d**) 1.50 T. The color bar next to the graphs represent the magnitude of the electron densities (n_e). In all these simulations, the initial plasma density was 5.0×10^{14} m^{-3}, the neutral gas pressure was $P = 6$ Pa, $T_e = 2.5$ eV, and $T_i = 0.025$ eV. It can be seen that at lower magnetic fields no filamentary pattern forms in the plasma. By increasing the magnetic field, the patterns appear in the plasma and by further increasing the magnetic field the patterns get narrower and closer to one another. The results are consistent with the experimental observations of the phenomenon.

figure that the cross-field mobility and diffusion coefficient of the ions increase with pressure up to a maximum point at a pressure that we shall call critical pressure. It is noticed that for this range of pressure, $\mu_{i\perp} \gg \mu_{e\perp}$, while $D_{i\perp} \geq D_{e\perp}$. It will be shown later that the cross-field component of the electric field in the bulk of a magnetized plasma can be non-zero. Therefore, it is the drift due to the electric field that guarantees the criterion of faster cross-field transport of the ions compared to the electrons which is crucial for pattern formation in magnetized plasmas. As a result, Eqs. 19–22 are describing the magnetized plasma as an activator-inhibitor system in which electrons are the activator and ions are the inhibitor. This also explains the disappearance of the filamentary patterns at high pressures as for pressures far beyond the critical pressure, neither of the required conditions for self-organization ($\mu_{i\perp} \gg \mu_{e\perp}$ or $D_{i\perp} \gg D_{e\perp}$) are satisfied.

In Eq. 19, the first two terms represent the self-activation by the electrons and the third term gives the suppression of the electrons production by the ions. The last terms in Eqs. 19 and 20 give the transport of electrons/ion parallel and perpendicular to the magnetic axis. The mobility and diffusion coefficients as well as other factors in these equations depend on the geometry of the plasma chamber and different discharge parameters. As long as the necessary conditions for self-organization are satisfied, variation of these parameters can produce different structures of self-organized patterns across the magnetic field lines.

Reproducing filamentary patterns through numerical simulation. Exact analytical solutions to Eqs. 19 and 20 cannot be obtained, and numerical simulations must be employed. Instead of directly solving these two equations, we solved their parent equations (Eqs. 5, 6, 7, 15, 17, and 18) using our 3D REctangular Model for mAgnetized Plasma Simulations (REMAPS) that has been extensively described in refs. [26,54].

REMAPS is a 3D fluid model in which the governing equations for the fluid motion of both electrons and ions are taken into account. Since the temperatures of electrons/ions are assumed to be constant in the model, it only solves Poisson's equation along with conservation of momentum and continuity equation for electrons and ions. The full set of equations in REMAPS for individual species α (= e, i - for electrons and ions) is given below:

$$\nabla^2 \varphi = \frac{\rho}{\varepsilon} \tag{23}$$

$$q_\alpha n_\alpha \left(\mathbf{E} + \mathbf{V}_\alpha \times \mathbf{B}\right) - \nabla \mathbf{P}_\alpha - m_\alpha n_\alpha \upsilon_{\alpha - n} \mathbf{V}_\alpha = m_\alpha n_\alpha \left(\frac{\partial \mathbf{V}_\alpha}{\partial \mathbf{t}} + (\mathbf{V}_\alpha . \nabla)\mathbf{V}_\alpha\right) \tag{24}$$

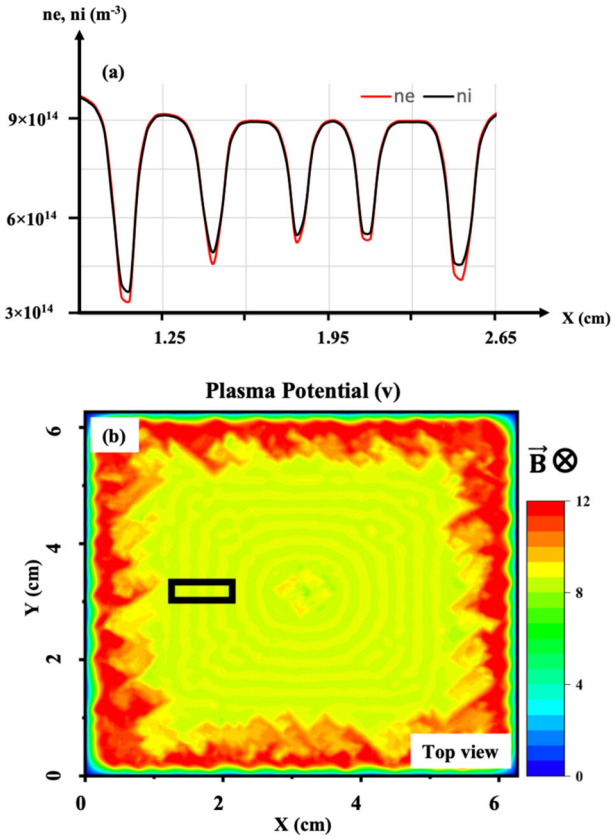

Fig. 8 The imbalance between electron and ion densities in the bulk of the magnetized plasma and its resultant potential structure. a Variation of electron/ion density in the regions indicated by the black boxes on Figs. 5a and 5b. (**b**) Top-view of the plasma potential profile in the simulation of a magnetized argon plasma in the middle of the plasma chamber (the color bar next to the graph represents the magnitude of the plasma potential). In the depletion regions of the filamentary pattern, the density of the ions is higher than the electrons. This density imbalance between electrons and ions results in a plasma potential profile similar to the density pattern. The region enclosed in the black box on **b** is magnified and explained in the next figure.

$$\boldsymbol{\Gamma_\alpha} = n_\alpha \mathbf{V_\alpha} \tag{25}$$

$$\frac{\partial n_\alpha}{\partial t} + \nabla\, \Gamma\boldsymbol{\alpha} = I - R \tag{26}$$

where ρ is the charge density given by $e(n_i - n_e)$, and ε is the electric permittivity, q_α is charge, n_α is density, **E** is electric field vector given by $-\nabla\boldsymbol{\varphi}$, $\mathbf{V_\alpha}$ is velocity vector, **B** is magnetic field vector, P_α is pressure, m_α is mass, $\upsilon_{\alpha\text{-}n}$ is collision frequency with neutral atoms, Γ_α is flux vector, I is ionization rate, and R is recombination rate of electrons and ions.

Figure 4 shows a schematic drawing of the simulated plasma chamber as the computational space in REMAPS. The background plasma conditions in the simulations were chosen to be similar to the experimental conditions that were measured in the MDPX device, but it is important to note that we are not performing a full simulation of the experiment. The chamber has grounded metal walls and is uniformly filled with electrons and ions (plasma) at target temperatures of 2.5 eV and 0.025 eV, respectively. The plasma gas is assumed to be Argon. A uniform magnetic field is applied to the plasma in negative Z direction. Through implementing this condition, the filamentary patterns form self-consistently in the computational space.

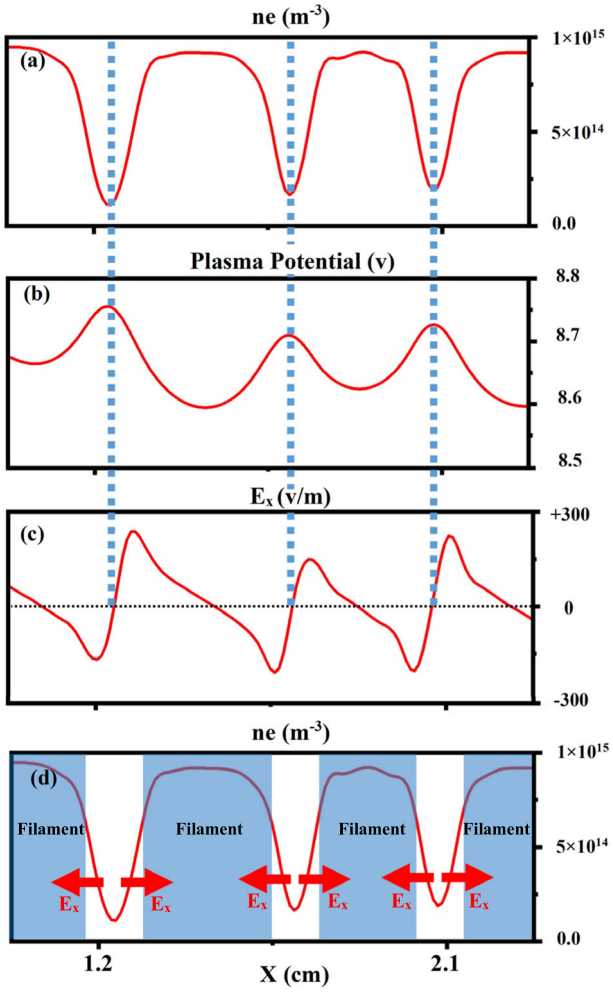

Fig. 9 The electron density, plasma potential, and electric field structure in the middle of the plasma chamber. a The electron density (n_e), (**b**) The plasma potential, and (**c**) the electric field ($\mathbf{E_x}$). The graphs are drawn along the X axis for the regions indicated by the black boxes on Figs. 5a, 5b and 8b. **d** gives the resultant of (**a**) and (**c**) in which the filament regions are masked with a dark color. **d** shows how the electric field points away (in negative and positive directions) from the depletion regions where the plasma potential peaks. This electric field structure maintains the filamentary patterns in magnetized plasmas.

Figure 5 displays the top-view of the electron/ion density profiles and side-view of the electron density profile in the middle of the plasma chamber. The initial uniform plasma density was set to be $5 \times 10^{14}\,\mathrm{m}^{-3}$, the neutral pressure was 9.0 Pa, and the applied magnetic field strength was 1.0 T. It can be seen in Fig. 5a, b that target-like filamentary patterns appear in the density profiles of electrons and ions. Similar to the experimental observations, these observed patterns in the simulations are extended through the plasma along the magnetic axis (see Fig. 5c). The filamentary patterns are more curved towards the center of the plasma chamber while they are rectangular near the sheath regions due to the imposed boundary condition by the rectangular walls. For future references, we call the regions of the patterned plasma with higher density compared to the initial plasma density "filament", while the regions in between the filaments with lower density will be called "depletion region".

By changing the initial conditions and the plasma parameter in the simulation, it is possible to generate different structures of filamentary patterns in the magnetized plasma. Figure 6 displays

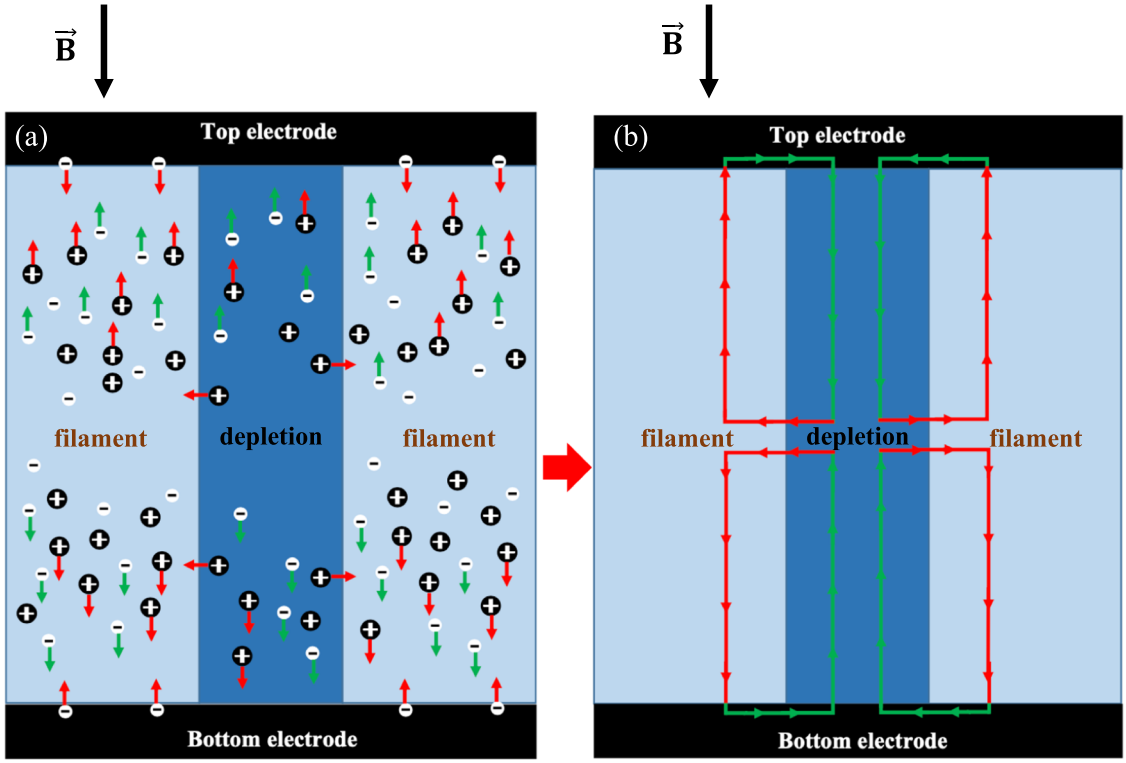

Fig. 10 Schematic drawing of the proposed formation mechanism for self-organized patterns in a low-pressure magnetized plasma. a Diffusion of the ions parallel and perpendicular to the magnetic field and the diffusion of the electrons parallel to the magnetic field in the filaments and depletion region. **b** Current channels created due to the parallel and cross-field diffusion of electrons and ion (note that both of the electrodes are assumed grounded in the model). In our proposed model, a depletion region is created by parallel diffusion of the electrons and parallel/cross-field diffusion of the ions from it. Also, the population of electrons/ions increases in a filament through ionization, cross-field diffusion of the ions from the depletion region, and the feedback of the diffused electrons from the depletion region through the electrodes as Simon currents. These transports of electron/ions create a closed loop of current that results in self-organization in magnetized plasmas. In **b**, the contribution of the electrons motion to this current loop (from depletion region to the electrodes and through the electrodes) is shown in green and the contribution of the ions motion and secondary electron emission from the electrodes into the filaments is shown in red.

variation of the filamentary patterns appearing in electron density profile by changing plasma parameters in the simulations compared to the results presented in Fig. 5. Therefore, we have been able to reproduce various filamentary patterns that were observed in the experiments on magnetized plasmas. By comparing these graphs to the experimental pictures that are displayed next to them, it can be seen that the simulation results are in good agreement with the experiments. Variation of the emerging patterns in a medium due to changing the initial conditions is a general characteristic of reaction-diffusion systems[30].

Moreover, Fig. 7 shows the variation of filamentation phenomenon in magnetized electric discharges with the strength of the applied magnetic field. It can be noticed in this figure that no significant pattern forms in the plasma exposed to 0.1 T magnetic field. By increasing the applied magnetic field to 0.25 T, filamentary patterns seem to start appearing in the plasma although the formation of the patterns in the plasma is not the dominant phenomenon. Further increasing the applied magnetic field results in the formation of filamentary patterns in the plasma and at higher magnetic fields, the filamentary patterns become narrower and closer to one another. These results were also observed in the experimental studies of the phenomenon reported by Schwabe et al.[23].

Stability of the self-organized structures in a strongly magnetized plasma. The activator-inhibitor model is mostly focused on the formation mechanism rather than the stability of the self-organized patterns[30]. On the other hand, considering the fact that electric discharges are very nonlinear media, it is compelling to discover the physics of the long-lived equilibrium of the filamentary structures in magnetized plasmas. While these patterns can be mobile or stationary, various sets of operating conditions can be found for which the patterns endure in the experiment or simulation much longer than characteristic time scales of the plasma such as time period of the plasma oscillations and electrons/ions gyro-rotation[22–27].

Although the filamentary patterns that appear in the electron and ion density profiles seem to be very similar (see Fig. 5a, b), these patterns are not exactly identical. It can be seen in Fig. 8a that in the depletion regions (regions at lower plasma density in the patterned plasma), the density of the electrons is less than that of the ions. This density imbalance results in a plasma potential structure that reproduces the spatial patterns observed in electron/ion density profiles as shown in Fig. 8b (also see Fig. 5a, b). By taking derivative of the plasma potential, the electric field vector in the bulk of the magnetized plasma can be obtained. Figure 9 shows the electron density, plasma potential, and the electric field along X axis in the middle of the plasma chamber for the region indicated by the black box on Figs. 5a, b and 8b. The electric field vector points away from the depletion regions (where the plasma potential peaks) in negative and positive directions. Therefore, unlike a regular unmagnetized electric discharge, a localized electric field exists in the bulk of a patterned magnetized plasma[52,53].

The presence of a patterned localized electric field in the bulk of the magnetized plasma is a very interesting finding which can explain the stability mechanism of the filamentary patterns in magnetized plasmas. For the ions, the transverse electric field that is oriented from the depletion region toward the filaments causes an electric force that counterbalances the force from the gradient of density that points from the filaments toward the depletion regions. On the other hand, although both gradients of density and electric field tend to push the electrons from the filaments towards the depletion region, the intense trapping of the electrons in the strong magnetic field maintains the filamentary structure in the magnetized plasma.

The self-organization mechanism in magnetized plasmas. Based on the results from the numerical simulations and the presented analytical description of low-pressure magnetized plasmas, we can propose a formation mechanism for filamentation phenomenon. The diffusion and mobility coefficients of the electrons/ions along the magnetic axis do not get affected by the magnetic field, and the transport of electrons parallel to the magnetic field occurs much faster than the ions. On the other hand, in the cross-field transport of the charged particles, the species with larger mass will have a higher mobility and diffusion coefficients (see Fig. 3). As a result, in a strongly magnetized plasma where electrons cannot travel perpendicular to the magnetic axis, ions can still have a non-zero transport across the field lines, mostly due to their much higher cross-field mobility compared to the electrons.

In a magnetized plasma, the electrons leave the ions behind through their fast diffusion along the magnetic axis and the whole plasma becomes electropositive. Accordingly, if there is a fluctuation in the plasma density, the density of ions in the fluctuation and the rest of the plasma will be different after the fast diffusion of the electrons parallel to the magnetic field. This will result in a transverse electric field that initiates the pattern formation by transporting the ions across the magnetic field lines. This transverse flux of the ions is enabled due to their much higher cross-field mobility compared to the electrons. Therefore, from the viewpoint of an activator-inhibitor model, the filamentary patterns get triggered in magnetized plasmas due to the disability of the activators (electrons) and ability of the inhibitors (ions) to travel perpendicular to the magnetic field in the presence of a local fluctuation/perturbation.

In order to establish regions of high and low density (filament and depletion regions), the electrons leave the depletion region parallel to the magnetic axis while ions leave the depletion region both parallel (largely) and perpendicular to the magnetic field (partially). The electrons that leave the depletion region to the walls of the plasma chamber parallel to the magnetic axis can be fed back into the filaments through secondary electron emission by traveling through the electrodes as Simon currents[55]. This transport of the electrons through the electrodes along with the transverse diffusion of the ions from the depletion regions to the filaments create a closed circuit that leads to the formation of filamentary patterns in magnetized plasmas. This process is schematically drawn in Fig. 10.

The formation process and stability mechanism proposed above suggest a reduced parallel diffusion for the electrons in the filaments and a continuous parallel diffusion in the depletion regions. The loss of more electrons to the top/bottom electrodes in the depletion regions compared to the filaments would mean that the direction of the electric field in the electrodes should be in opposite direction of horizontal electric field in the bulk of plasma. Figure 11 displays the horizontal electric field in the middle of the top electrode and in the bulk of the plasma along X axis which is consistent with the expected orientation. Since the direction of the electric field in the bulk of the plasma is from the depletion region to the filaments, the observed orientation of the electric field would create a short-circuit giving a closed current path in the magnetized plasma. This transport mechanism of charged particles in magnetized electric discharges is known as a Simon current[55].

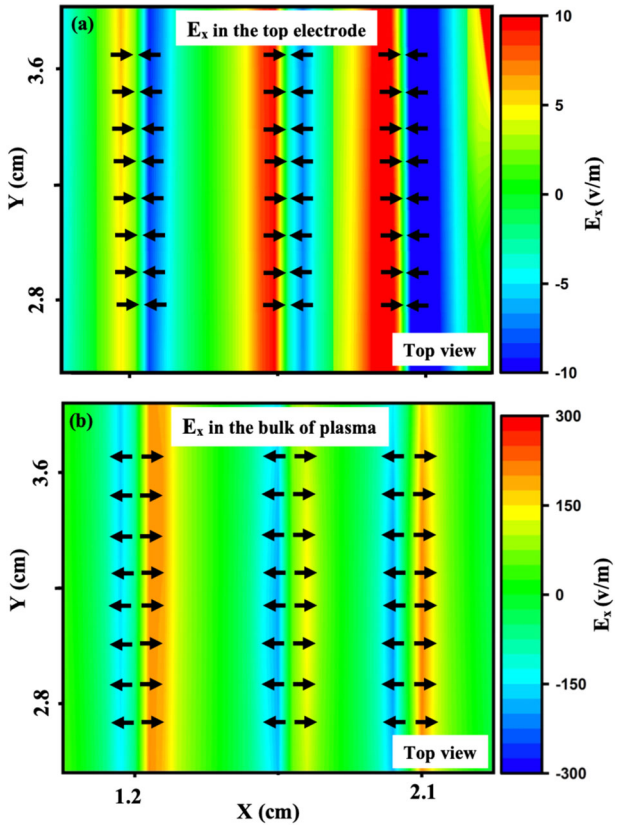

Fig. 11 Orientation of the horizontal element of electric field (E_x) along X axis. a In the middle of the top electrode, and (**b**) in the bulk of the plasma. The color bars next to the graphs represent the magnitude of the electric field element ($\mathbf{E_x}$). The black arrows on the graphs display the orientation of the electric field. These electric field elements are pointing in opposite direction, confirming the presence of a closed loop of current in the plasma as it was proposed and depicted in Fig. 10b.

Data availability

The datasets generated and/or analyzed during the current study are available from the corresponding author on reasonable request.

Received: 11 May 2021; Accepted: 4 August 2023;
Published online: 19 August 2023

References

1. Cross, M. & Greenside, H. *Pattern Formation and Dynamics in Nonequilibrium Systems. Pattern Formation and Dynamics in Nonequilibrium Systems* (Cambridge University Press, 2009).
2. Schuocker, D. Improved model for anode spot formation in vacuum arcs. *IEEE Trans. Plasma Sci* **7**, 209–216 (1979).
3. Baksht, F. G., Dyuzhev, G. A., Mitrofanov, N. K. & Shkol'nik, S. M. Experimental investigation of the anode region of a free-burning atmospheric-pressure inert-gas arc. II. Intermediate current regime—multiple anode constriction. *Tech. Phys.* **42**, 35–38 (1997).

4. Yang, G. & Heberlein, J. Instabilities in the anode region of atmospheric pressure arc plasmas. *Plasma Sources Sci. Technol* **16**, 765–773 (2007).
5. Schoenbach, K. H., Moselhy, M. & Shi, W. Self-organization in cathode boundary layer microdischarges. *Plasma Sources Sci. Technol* **13**, 177–185 (2004).
6. Purwins, H.-G. Self-organized patterns in planar low-temperature AC gas discharge. *IEEE Trans. Plasma Sci* **39**, 2112–2113 (2011).
7. Purwins, H.-G. J. & Berkemeier, J. Self-organized patterns in planar low-temperature DC gas discharge. *IEEE Trans. Plasma Sci* **39**, 2116–2117 (2011).
8. Ebert, U. & Arrayás, M. *Pattern Formation in Electric Discharges*. p. 270–282 (Springer Nature, 2001).
9. Li, B. & Ouyang, J. Comparing investigation of pattern formation in glow and streamer DBD. *Phys. Plasmas* **23**, 113509 (2016).
10. Chirokov, A. et al. A study of two-dimensional microdischarge pattern formation in dielectric barrier discharges. *Plasma Chem. Plasma Process.* **26**, 127–135 (2006).
11. Abolmasov, S. N., Tachibana, K. & Shirafuji, T. Mechanisms of pattern formation in dielectric barrier discharges. *IEEE Trans. Plasma Sci.* **39**, 2090–2091 (2011).
12. Babaeva, N. Y. & Kushner, M. J. Self-organization of single filaments and diffusive plasmas during a single pulse in dielectric-barrier discharges. *Plasma Sources Sci. Technol.* **23**, 065047 (2014).
13. Trelles, J. P. Pattern formation and self-organization in plasmas interacting with surfaces. *J. Phys. D Appl. Phys.* **49**, 393002 (2016).
14. Dimitrakellis, P. & Gogolides, E. Atmospheric plasma etching of polymers: a palette of applications in cleaning/ashing, pattern formation, nanotexturing and superhydrophobic surface fabrication. *Microelectron. Eng.* **194**, 109–115 (2018).
15. Jaiswal, S. et al. Effect of growing nanoparticle on the magnetic field induced filaments in a radio-frequency Ar/C 2 H 2 discharge plasma. *Jpn J. Appl. Phys.* **59**, SHHC07 (2020).
16. Dai, L., Griesser, H. J. & Mau, A. W. H. Surface modification by plasma etching and plasma patterning. *J. Phys. Chem. B* **101**, 9548–9554 (1997).
17. Kwon, T., Kan, H.-C., Oehrlein, G. S. & Phaneuf, R. J. Transient roughening behaviour and spontaneous pattern formation during plasma etching of nanoporous silica. *Nanotechnology* **18**, 055305 (2007).
18. Motrescu, I., Ciolan, M. A., Sugiyama, K., Kawamura, N. & Nagatsu, M. Use of pre-ionization electrodes to produce large-volume, densely distributed filamentary dielectric barrier discharges for materials surface processing. *Plasma Sources Sci. Technol.* **27**, 115005 (2018).
19. Chen, Z., Zhang, S., Levchenko, I., Beilis, I. I. & Keidar, M. In vitro demonstration of cancer inhibiting properties from stratified self-organized plasma-liquid interface. *Sci. Rep.* **7**, 12163 (2017).
20. Vladimirov, S. V. & Ostrikov, K. Dynamic self-organization phenomena in complex ionized gas systems: new paradigms and technological aspects. *Phys. Rep.* **393**, 175–380 (2004).
21. Genco, F. & Hassanein, A. Modeling and simulation of the erosion damage in tokamak devices during plasma instabilities. in *2011 Abstracts IEEE International Conference on Plasma Science* 1–1 https://doi.org/10.1109/PLASMA.2011.5993082 (IEEE, 2011).
22. Konopka, U. Complex Plasmas in Strong Magnetic Field Environments. in *AIP Conference Proceedings* **799** 181–184 (AIP, 2005).
23. Schwabe, M., Konopka, U., Bandyopadhyay, P. & Morfill, G. E. Pattern formation in a complex plasma in high magnetic fields. *Phys. Rev. Lett.* **106**, 215004 (2011).
24. Menati, M., Thomas, E. & Kushner, M. J. Filamentation of capacitively coupled plasmas in large magnetic fields. *Phys. Plasmas* **26**, 063515 (2019).
25. Thomas, E. et al. Pattern formation in strongly magnetized plasmas: observations from the magnetized dusty plasma experiment (MDPX) device. *Plasma Phys. Control. Fusion* **62**, 014006 (2020).
26. Menati, M., Rasoolian, B., Thomas, E. & Konopka, U. Experimental observation and numerical investigation of filamentary structures in magnetized plasmas. *Phys. Plasmas* **27**, 022101 (2020).
27. Menati, M., Konopka, U., & Thomas, E. Variation of filamentation phenomenon in strongly magnetized plasma with various discharge parameters, *Contrib. Plasma Phys.* **61**, e202100083 (2021).
28. Thomas, E., Merlino, R. L. & Rosenberg, M. Magnetized dusty plasmas: the next frontier for complex plasma research. *Plasma Phys. Control. Fusion* **54**, 124034 (2012).
29. Thomas, E. et al. The magnetized dusty plasma experiment (MDPX). *J. Plasma Phys.* **81**, 345810206 (2015).
30. Turing, A. M. The chemical basis of morphogenesis. *Philos. Trans. R. Soc. Lond. B Biol. Sci.* **237**, 37–72 (1952).
31. Huang, S.-W. et al. Globally stable microresonator turing pattern formation for coherent high-power THz radiation on-chip. *Phys. Rev. X* **7**, 041002 (2017).
32. Gierer, A. & Meinhardt, H. A theory of biological pattern formation. *Kybernetik* **12**, 30–39 (1972).
33. Gierer, A. Generation of biological patterns and form: some physical, mathematical, and logical aspects. *Prog. Biophys. Mol. Biol.* **37**, 1–47 (1981).
34. Meinhardt, H. Models of biological pattern formation. *Acad. Press. London* https://doi.org/10.1016/S0070-2153(07)81001-5 (1982).
35. Kessler, M. A. Self-organization of sorted patterned ground. *Science (80-.)* **299**, 380–383 (2003).
36. Cartwright, J. H. E., Checa, A. G., Escribano, B. & Sainz-Diaz, C. I. Spiral and target patterns in bivalve nacre manifest a natural excitable medium from layer growth of a biological liquid crystal. *Proc. Natl. Acad. Sci. USA* **106**, 10499–10504 (2009).
37. Callegari, T., Bernecker, B. & Boeuf, J. P. Pattern formation and dynamics of plasma filaments in dielectric barrier discharges. *Plasma Sources Sci. Technol.* **23**, 054003 (2014).
38. Vanag, V. K. Inwardly rotating spiral waves in a reaction-diffusion system. *Science (80-.)* **294**, 835–837 (2001).
39. Bao, H. et al. Turing patterns in a fiber laser with a nested microresonator: Robust and controllable microcomb generation. *Phys. Rev. Res.* **2**, 023395 (2020).
40. Lengyel, I. & Epstein, I. R. Turing structures in simple chemical reactions. *Acc. Chem. Res.* **26**, 235–240 (1993).
41. Tompkins, N. et al. Testing Turing's theory of morphogenesis in chemical cells. *Proc. Natl. Acad. Sci. USA* **111**, 4397–4402 (2014).
42. Maini, P. K., Painter, K. J. & Nguyen Phong Chau, H. Spatial pattern formation in chemical and biological systems. *J. Chem. Soc. Faraday Trans.* **93**, 3601–3610 (1997).
43. Kondo, S. & Miura, T. Reaction-diffusion model as a framework for understanding biological pattern formation. *Science (80-)* **329**, 1616–1620 (2010).
44. Landge, A. N., Jordan, B. M., Diego, X. & Müller, P. Pattern formation mechanisms of self-organizing reaction-diffusion systems. *Dev. Biol.* **460**, 2–11 (2020).
45. Sherratt, J. A. Turing Patterns in Deserts. in *Lecture Notes in Computer Science (including subseries Lecture Notes in Artificial Intelligence and Lecture Notes in Bioinformatics)* p. 667–674 (Springer Nature, 2012).
46. Meinhardt, H. The algorithmic beauty of sea shells, xi, 204p. Berlin: Springer-Verlag, 1995. Price DM 78.00. *J. Mar. Biol. Assoc. UK* **75**, 1004–1004 (1995).
47. Ermentrout, B. & Lewis, M. Pattern formation in systems with one spatially distributed species. *Bull. Math. Biol.* **59**, 533–549 (1997).
48. Satnoianu, R. A., Menzinger, M. & Maini, P. K. Turing instabilities in general systems. *J. Math. Biol.* **41**, 493–512 (2000).
49. Biancalani, T., Fanelli, D. & Di Patti, F. Stochastic tring patterns in the Brusselator model. *Phys. Rev. E* **81**, 046215 (2010).
50. Segel, L. A. & Jackson, J. L. Dissipative structure: an explanation and an ecological example. *J. Theor. Biol.* **37**, 545–559 (1972).
51. Busiello, D. M., Planchon, G., Asllani, M., Carletti, T. & Fanelli, D. Pattern formation for reactive species undergoing anisotropic diffusion. *Eur. Phys. J. B* **88**, 222 (2015).
52. Lieberman, M. A. & Lichtenberg, A. J. *Principles of Plasma Discharges and Materials Processing. Principles of Plasma Discharges and Materials Processing.* 2nd edn (John Wiley & Sons, Inc., 2005).
53. Chen, F. F. *Introduction to Plasma Physics and Controlled Fusion. Introduction to Plasma Physics and Controlled Fusion* (Springer International Publishing, 2016).
54. Menati, M. et al. Experimental Observation and Numerical Investigation of Imposed Pattern Formation in Magnetized Plasmas by a Wide Wire Mesh. *Plasma Sources Sci. Technol.* **29**, (2020).
55. Simon, A. Ambipolar diffusion in a magnetic field. *Phys. Rev.* **98**, 317–318 (1955).

Acknowledgements

The authors would like to thank Dr. Thakur from Auburn University Physics Department for his collaboration in preparing the responses to the reviewers' comments and Dr. Sharma and Dr. Bandyopadhyay from Institute for Plasma Research, Bhat, Gandhinagar (Gujarat), India, for the insightful physics discussions. This work was supported by funds from the National Science Foundation EPSCoR program (OIA-1655280, OIA-2148653), NASA / Jet Propulsion Laboratory (JPL-RSA 1571699), and US Department of Energy (SC-0019176).

Author contributions

M.M. was the main developer of the numerical model and the primary author of the manuscript. S.W. partially contributed to the experimental results. B.R. assisted in developing the numerical model. E.T. and U.K. supervised the project, partially contributed to the experimental results, and edited/reviewed the manuscript.

Competing interests
The authors declare no competing interests.

Additional information
Correspondence and requests for materials should be addressed to Mohamad Menati.

Peer review information *Communications Physics* thanks the anonymous reviewers for their contribution to the peer review of this work.

Reprints and permission information is available at http://www.nature.com/reprints

Publisher's note Springer Nature remains neutral with regard to jurisdictional claims in published maps and institutional affiliations.